Journal of
Synchrotron
Radiation

ISSN 1600-5775

Received 14 June 2013
Accepted 20 October 2013

A reaction cell for time-resolved *in situ* XAS studies during wet chemical synthesis: the $Cu_2(OH)_3Cl$ case

Jocenir Boita,[a] Maria do Carmo Martins Alves[b] and Jonder Morais[a]*

[a]Instituto de Física, Universidade Federal do Rio Grande do Sul (UFRGS), Avenida Bento Gonçalves 9500, Bairro Agronomia, CP 15051, CEP 91501-970, Porto Alegre, RS, Brazil, and [b]Instituto de Química, Universidade Federal do Rio Grande do Sul (UFRGS), Avenida Bento Gonçalves 9500, Bairro Agronomia, CP 15003, CEP 91501-970, Porto Alegre, RS, Brazil. *E-mail: jonder@if.ufrgs.br

The use of *in situ* time-resolved dispersive X-ray absorption spectroscopy (DXAS) to monitor the formation of $Cu_2(OH)_3Cl$ particles in an aqueous solution is reported. The measurements were performed using a dedicated reaction cell, which enabled the evolution of the Cu *K*-edge X-ray absorption near-edge spectroscopy to be followed during mild chemical synthesis. The formed $Cu_2(OH)_3Cl$ particles were also characterized by synchrotron-radiation-excited X-ray photoelectron spectroscopy, X-ray diffraction and scanning electron microscopy. The influence of polyvinylpyrrolidone (PVP) on the electronic and structural properties of the formed particles was investigated. The results indicate clearly the formation of $Cu_2(OH)_3Cl$, with or without the use of PVP, which presents very similar crystalline structures in the long-range order. However, depending on the reaction, dramatic differences were observed by *in situ* DXAS in the vicinities of the Cu atoms.

Keywords: $Cu_2(OH)_3Cl$; DXAS; X-ray absorption; *in situ*; copper.

1. Introduction

X-ray absorption spectroscopy (XAS) has been employed widely to characterize the structural and electronic properties of materials (Koningsberger & Prins, 1988). In addition, XAS enables atom-specific *in situ* measurements to be performed, which allow the observation of the changes that occur in the electronic structure of a chemical element, the local geometry around the probed atom, its oxidation state, the local disorder, and the nature and distance of neighboring atoms. The variation of XAS called *in situ* dispersive X-ray absorption spectroscopy (DXAS) provides the momentum to obtain accurate information during a reaction process (Tolentino *et al.*, 2005). It allows time-resolved measurements of the electronic structure, thereby providing additional details on the formation mechanism. In a recent study (Bernardi *et al.*, 2010), *in situ* DXAS was applied to follow the formation of Pt nanoparticles under hydrogen reduction of commercial PtO_2. Moreover, Adriaens *et al.* (2009) made use of time-resolved *in situ* XAS at the Cu *K*-edge to study corrosion on archaeological cupreous artifacts recovered from marine environments. This was achieved by observing changes in the XANES (X-ray absorption near-edge spectroscopy) and extended X-ray absorption fine structure (EXAFS) regions of a copper sample under simulated corrosion conditions. In addition, *in situ* time-resolved XAS was applied to understand the role of polyvinylpyrrolidone (PVP) in the formation mechanism of copper nanoparticles (Nishimura *et al.*, 2009). PVP is used frequently as a capping agent to control the size and structure of particles in various types of chemical synthesis.

In recent years, micro- and nano-scale inorganic particles have triggered considerable research based on their electronic, mechanical and optical properties. In particular, copper-based particles have been used as catalysts, batteries, gas sensors, biosensors and transistors (Tamaki *et al.*, 1998; Zheng *et al.*, 2000; Chen *et al.*, 2003; Chowdhuri *et al.*, 2004; Wang *et al.*, 2007). For example, a number of studies of basic copper (II) chlorides have been undertaken. Reports in the area of photocatalysis have revealed that $Cu_2(OH)_3Cl$ [copper trihydroxyl chloride or copper (II) oxychloride], immersed in reduced graphene oxide, displays excellent catalytic performance in the degradation of rhodamine B under visible-light irradiation (Park *et al.*, 2007).

The synthesis of $Cu_2(OH)_3Cl$ usually occurs under harsh conditions, for instance by the hydrothermal reaction of $CuCl_2$, NH_2CONH_2 and NaOH at 394 K (Jia *et al.*, 2009), resulting in the formation of particles with an average size of 5–10 µm. Similarly, spherical $Cu_2(OH)_3Cl$ aggregates have been synthesized hydrothermally (Lee *et al.*, 2007) using $CuCl_2.2H_2O$, urea, 1-octanesulfonic acid sodium salt, sodium hydroxide and water. Although the shape and size of $Cu_2(OH)_3Cl$ particles have been controlled, there is still the need for a detailed description of the structural and electronic evolution in the vicinity of the Cu atoms during $Cu_2(OH)_3Cl$ formation, and *in situ* XAS can shed light on this.

An important aspect to be considered for *in situ* XAS (or DXAS) measurements is the use of reactors (or cells) that are compatible with the investigated sample and its reaction environment. Various types of reactors for *in situ* XAS measurements have been reported, the most common being those for solid samples, but few are designed to monitor the formation of particles in liquids.

In the present work the formation of $Cu_2(OH)_3Cl$ particles in an aqueous solution under mild conditions was monitored by *in situ* DXAS. We have designed and built a dedicated reaction cell, which

was used to monitor the evolution of the Cu *K*-edge XANES for two chemical conditions: in the presence and in the absence of PVP. XANES spectra were collected continuously throughout the syntheses providing the bulk-sensitive information. The freshly formed particles were characterized by synchrotron-radiation-excited X-ray photoelectron spectroscopy (XPS) in order to probe their surface chemical environment. Complementary X-ray diffraction (XRD) and scanning electron microscopy (SEM) provided long-range-order structural information and morphology, respectively.

2. Experimental

2.1. Reaction cell

The reaction cell used for the *in situ* synchrotron experiments and its other components is shown in Fig. 1. It consists of a supporting screw, cap, borosilicate glass vessel, windows and adjustable pistons. The supporting screw is used to attach the assembly to the motorized (*XYZ*) table of the beamline. The cell itself consists of a modified Schott Duran bottle that houses two hollow Teflon pistons. Each piston has a Kapton window attached at one end, and by moving the pistons in or out of the cell one may adjust the probed thickness of the liquid (*i.e.* the X-ray path) from 0.1 to 12 mm and, therefore, optimize the edge jump. A magnetic stirrer can be placed under the reaction cell to rotate a magnetic bar placed in the solution, homogenizing it during the measurements. This set-up allows the spectra of a solution, which can be heated up to 423 K, to be acquired.

2.2. Sample synthesis

The $Cu_2(OH)_3Cl$ particles were prepared using copper (II) chloride (Carlo Erba), sodium citrate (Sigma-Aldrich), ascorbic acid (Vetec) and PVP (Aldrich). The synthesis, conducted at room temperature, took place inside the reactor under two different conditions: in the presence of PVP (Reaction-I) and without PVP (Reaction-II).

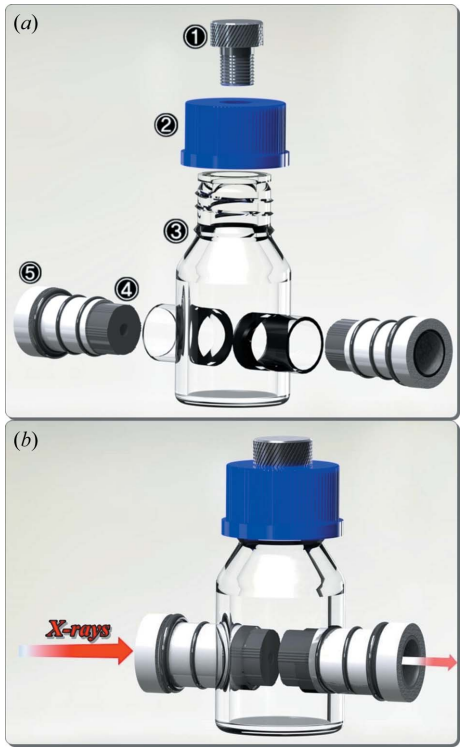

Figure 1
(*a*) Reaction cell components: supporting screw (1), cap (2), borosilicate glass vessel (3), Kapton windows (4), and adjustable pistons (5). (*b*) The fully assembled cell.

2.2.1. Reaction-I. Four aqueous solutions were prepared separately using deionized (DI) water: 2 ml of 1.5 mol L^{-1} $CuCl_2.2H_2O$, 2 ml of 1.5 mol L^{-1} $C_6H_5O_7Na_3.2H_2O$, 2 ml of 0.8 mol L^{-1} $(C_6H_9NO)_n$ (n = 40000) and 10 ml of 1.5 mol L^{-1} $C_6H_8O_6$. The first three solutions were then mixed in the reactor under stirring. The ascorbic acid solution (VC) was added later to start the reaction. This reaction was monitored for 174.7 min, with t = 0 s corresponding to the instant when the VC was added.

2.2.2. Reaction-II. Three aqueous solutions were prepared using DI water: 3 ml of 0.5 mol L^{-1} $CuCl_2.2H_2O$ (Carlo Erba), 3 ml of 1.0 mol L^{-1} $C_6H_5O_7Na_3.2H_2O$ (Sigma) and 15 ml of 1.0 mol L^{-1} $C_6H_8O_6$ (Vetec). The first two solutions were mixed in the reaction cell under stirring. The VC was added to start the reaction, which was monitored for 174.6 min, with t = 0 s corresponding to the instant when the VC was added.

At the end of each reaction the solutions were centrifuged. The precipitates were collected and washed thoroughly with DI water and isopropyl alcohol, followed by additional centrifugation. The particles were dried in air and stored in a glove box prior to the *ex situ* characterizations by XPS, XRD and SEM.

2.3. *In situ* and e*x situ* characterizations

The DXAS measurements were performed at the LNLS (Brazilian Synchrotron Light Laboratory) DXAS beamline (Tolentino *et al.*, 2005). The monochromator consisted of a curved Si (111) crystal (dispersive polychromator) that focuses the beam in the horizontal plane down to about 200 µm and in the vertical plane to about 500 µm. The detector was a position-sensitive CCD camera. The reactor was placed in the beamline at the X-ray focal point. The measurements were performed at the Cu *K*-edge.

The freshly prepared (dried) $Cu_2(OH)_3Cl$ particles were also analyzed at the SXS beamline (Tolentino *et al.*, 1998) endstation (also at LNLS) for XPS measurements. The spectra were collected using an InSb (111) double-crystal monochromator at a fixed photon energy of 1840 eV. The hemispherical electron analyzer (Phoibos 150MCD-9) was set with pass energy of 30 eV and the energy step was 0.1 eV with an acquisition time of 500 ms per point. The use of synchrotron radiation provided spectra with intense signals and an excellent overall resolution of about 0.44 eV. The base pressure inside the chamber was about 1.3×10^{-9} mbar. The monochromator photon energy calibration was performed at the Si *K*-edge (1839 eV). An additional calibration of the analyzer's energy was performed using a standard Ag foil (Ag $3d_{5/2}$ peak at 368.3 eV). We also considered the C 1*s* peak value of 284.5 eV as a reference to verify possible charging effects. The accuracy of the experimental binding energy scale was ±0.1 eV. The samples were placed on carbon tape and the XPS measurements were obtained at a 45° take-off angle at room temperature. *XPS Peak* version 4.1 was used to fit the XPS results. All peaks were adjusted using a Shirley-type background and an asymmetric Gaussian–Lorentzian sum function (30% Lorentzian contribution). The full width at half-maximum of the XPS components was allowed to vary by 0.4 eV around their typical values.

The XRD measurements were performed using a Siemens D500 with Cu K_α radiation (17.5 mA, 40 kV and λ = 1.54 Å). The diffraction peaks were indexed using the Crystallographica Search-Match (version 2.1.1.1), AMCSD and ICSD databases. The SEM images were obtained using a Jeol JSM-6060, operating at 20 kV.

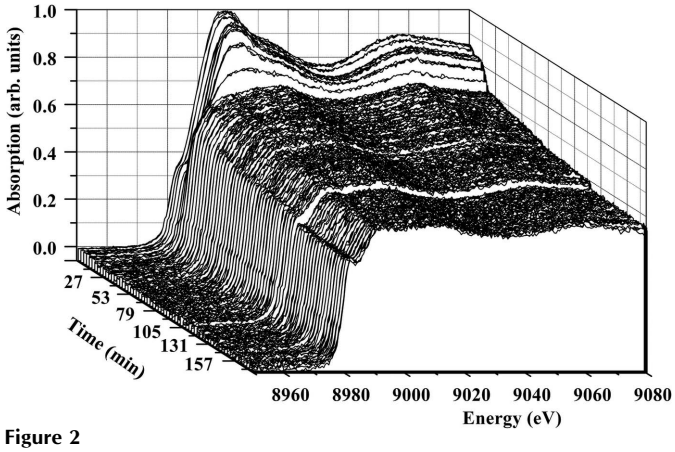

Figure 2
Evolution of the Cu *K*-edge during Reaction-I, starting at the addition of the ascorbic acid solution (t = 0 s). The accumulation time for each XANES spectrum was 1.6 s, for a total reaction time of 175.7 min.

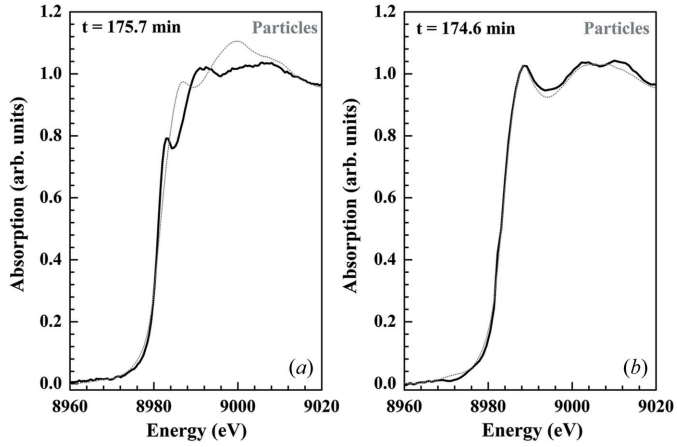

Figure 4
Comparison between the final XANES spectra (full lines) of (*a*) Reaction-I, (*b*) Reaction-II and the XANES of their respective isolated particles (dotted lines).

3. Results

3.1. *In situ* DXAS

Fig. 2 shows the evolution of the *in situ* XANES spectra for Reaction-I. The time required for accumulation of each spectrum was approximately 1.6 s, and about 6700 spectra were collected. The evolution suggests significant changes as a function of the reaction time. To visualize the changes better, Fig. 3(*a*) displays some of the XANES curves that are representative of Reaction-I kinetics along with the spectra of reference compounds.

The XANES spectrum for t = 0 s does not resemble that of $CuCl_2$ + sodium citrate (SC) nor that of $CuCl_2$ + SC + PVP. It presents clearly two electronic transitions in the absorption edge, named features *A* and *B*. Furthermore, taking into account the relative height of these transitions, we may say that they correspond to a distorted octahedral geometry. The lowest energy is due to a $1s \rightarrow 4p_z$ transition, and the highest energy transition $1s \rightarrow 4p_z, 4p_y$ is characteristic of square-planar geometries. For t = 13.1 min one observes an increase in the intensity of the first transition and a decrease of the second. At t = 15.9 min the spectrum is much distorted and the only observable feature is the characteristic step-like shape of the absorption edge. After t = 131 min the XANES curve changed and presented two new features: *C* and *D*. The relative position of the first transition and the general shape of the spectrum are consistent with the spectra of ML_4X_2 complexes, where *M* is the metal, *L* is the ligand and *X* another ligand at a longer distance (Cartier, 1988). The longer *M*–*X* distance has an effect similar to that observed in a square-planar geometry, where the spread of the ligands on the *z*-axis leads to preferential stabilization of the p_z orbital.

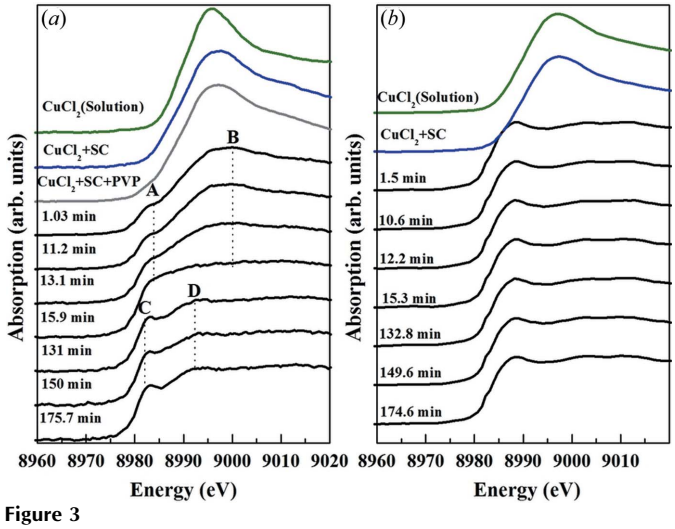

Figure 3
Collected Cu *K*-edge XANES spectra: (*a*) Reaction-I and (*b*) Reaction-II. XANES of reference solutions are also displayed.

We also monitored the evolution of the XANES spectra during Reaction-II. In this experiment we chose to improve the statistics by using a larger acquisition time per point. The accumulation for each XANES spectrum was approximately 90 s, with an excellent signal-to-noise ratio. Fig. 3(*b*) displays some curves collected during the Reaction-II kinetics, along with the XANES spectra of reference compounds. The two XANES spectra are quite similar and do not resemble any of the reference curves shown in Fig. 3. In particular, these curves present similar features to those found in XANES spectra obtained from Cu-based minerals (Dowsett *et al.*, 2008), especially that of a mineral called paratacamite, whose chemical formula is $Cu_2(OH)_3Cl$ (Fleet, 1975).

After the *in situ* DXAS experiment, the formed particles were collected, washed and dried (in air) prior to additional XANES measurements. Fig. 4 shows a comparison of the final spectrum acquired *in situ* with the spectrum of the particles obtained from Reactions-I (*a*) and II (*b*). For Reaction-I we believe that the differences in the XANES features indicate that the washing process removes some of the PVP, altering the chemical environment of the Cu atoms in the solid. In the case of Reaction-II the features of the two spectra are quite similar, indicating that in the absence of PVP the procedures to extract the precipitate from the solution do not affect the chemical environment of Cu. The lack of standard samples similar to the formed particles is a difficulty for the direct association of the XANES spectra obtained in each reaction with a particular type of structure.

3.2. XPS

The Cu 2*p* XPS spectra of the particles formed by both reactions are shown in Fig. 5. Curves (*a*) and (*b*) are different in shape as well as in intensity, indicating that the bonding type of Cu might be distinct. The two main peaks correspond to the Cu $2p_{1/2}$ and $2p_{3/2}$ doublet with a spin-orbit splitting of around 19.80 eV. The Cu $2p_{3/2}$ region was fitted in order to understand the chemical states of the Cu atoms in each case.

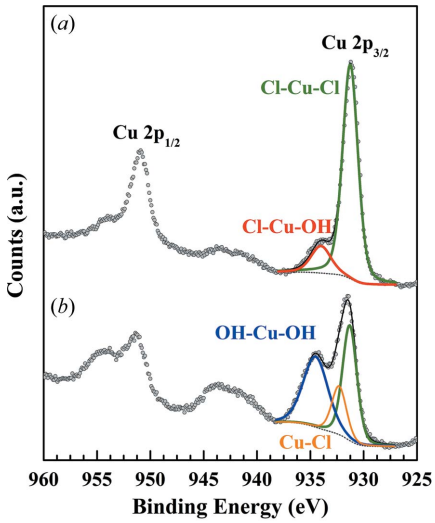

Figure 5
Cu 2*p* XPS spectrum of the particles synthesized using (*a*) Reaction-I and (*b*) Reaction-II, indicating the presence of Cl–Cu–Cl, Cl–Cu–OH, OH–Cu–OH and Cu–Cl bonds.

For Reaction-I, the Cu $2p_{3/2}$ presents two chemical components at 931.3 eV and 934.0 eV binding energies, which correspond to Cl–Cu–Cl and Cl–Cu–OH bonds, respectively. These bonds observed here are consistent with the presence of $Cu_2(OH)_3Cl$ (Han *et al.*, 2003).

The XPS analysis of the Cu $2p_{3/2}$ region of the particles formed by Reaction-II presented three chemical components. In addition to the Cu–Cu–Cl bonds at 931.3 eV, components at 932.3 eV (Cu–Cl bonds) and 934.5 eV (OH–Cu–OH bonds) were observed.

3.3. XRD

The XRD pattern of the particles obtained from Reaction-I and Reaction-II (Fig. 6*a*) were properly indexed according to the crystallographic database (Fig. 6*b*), and correspond to $Cu_2(OH)_3Cl$ in two phases (AMCSD 10032 and 9525). Particularly in the case of particles obtained from Reaction-II (without PVP), we may also observe additional peaks identified due to the presence of CuCl (ICSD 60711). These particles are clearly less ordered than those obtained in Reaction-II, as ascertained by their less intense diffraction peaks. In both cases one observes a background, which is a contribution from amorphous phases.

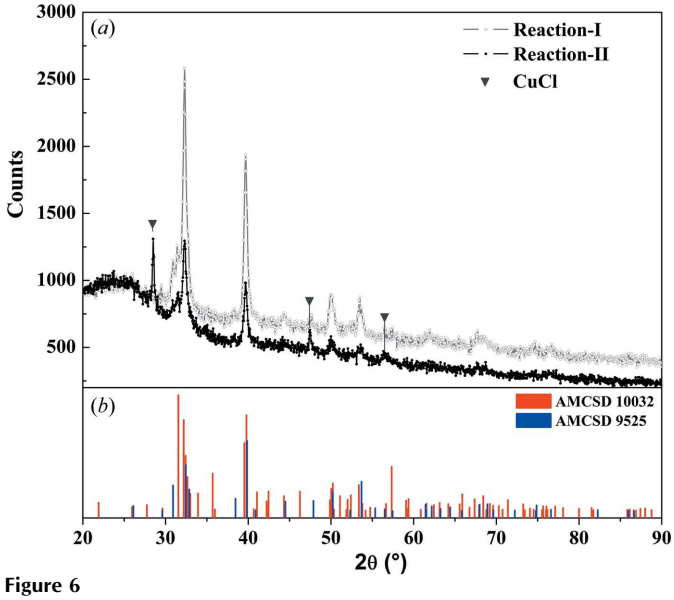

Figure 6
(*a*) Diffractogram of the particles formed in Reaction-I and Reaction-II. (*b*) The indexed peaks correspond to $Cu_2(OH)_3Cl$ in two phases. The inverted triangles indicate the CuCl peaks observed for the Reaction-II particles.

3.4. SEM

Figs. 7(*a*) and 7(*b*) present SEM images of the particles formed by Reactions-I and II, respectively. PVP was used in Reaction-I to encapsulate the aggregates during its formation and to control its final size. As a result, the images present two major types of morphology. The smaller particles present are ∼300 nm in size, but are without a definite form. The larger particles have a pyramidal shape in the micrometer range. The size distribution varies from hundreds of nanometers to micrometers. In the case of Reaction-II (Fig. 7*b*) the morphology may be described as shapeless with a size in the micrometer range.

4. Discussion

The *in situ* DXAS results indicated first of all that the proposed reactor is quite functional, allowing reactions to be monitored *via* the evolution of the Cu *K*-edge XANES spectrum, from its initial state in the form of Cu^{2+} in solution, until the formation of a solid copper compound. In the case of Reaction-II, the quality of the signal was improved by using longer acquisition times. Nevertheless, it was noticeable that the evolution of the electronic structure of the Cu is different than that for Reaction-I, which is attributed to the absence of PVP in the latter.

The XANES spectra of the formed particles in Reactions I and II are distinct, showing that there are differences in the short-range order, *i.e.* in the vicinity of the Cu atoms. Furthermore, the surface information provided by the XPS spectra of these same particles confirms that the chemical environment of the Cu atoms is distinct and characteristic of $Cu_2(OH)_3Cl$. According to the XRD results, which provide a long-range crystalline order, both reactions formed $Cu_2(OH)_3Cl$. Reaction-II particles present additional CuCl diffraction peaks.

The explanation for all of the above results is that both reactions resulted in the formation of two forms of $Cu_2(OH)_3Cl$: one called

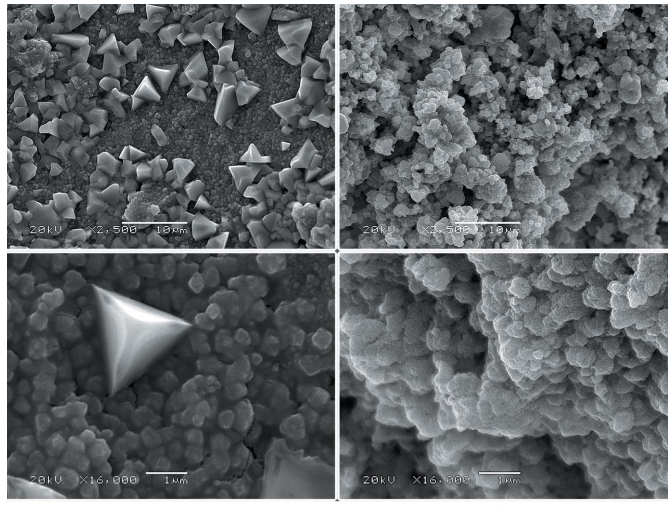

(*a*) (*b*)

Figure 7
SEM images of the particles formed by (*a*) Reaction-I and (*b*) Reaction-II.

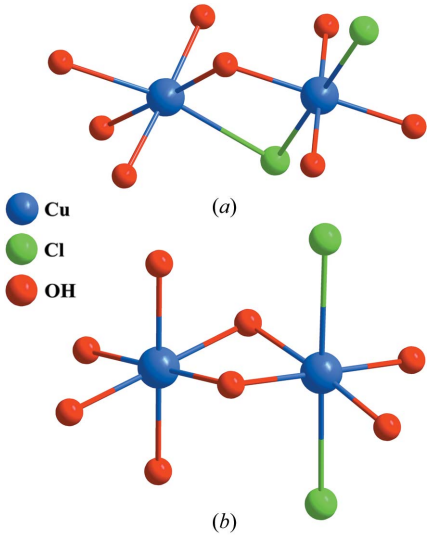

Figure 8
Possible octahedral Cu sites in two $Cu_2(OH)_3Cl$ polymorphs: (*a*) atacamite and (*b*) paratacamite.

atacamite (orthorhombic, space group *Pnma*) and the other called paratacamite (trigonal, space group $R\bar{3}$). Both have very similar crystalline structures and XRD patterns, but present dramatic differences in the local order around the Cu atoms, which are illustrated in Fig. 8. In the case of atacamite the Cu atoms have two possible octahedral sites. In one of the sites the Cu is surrounded by four OH^- (planar) at a shorter distance (2.0 Å) and two Cl atoms further away (2.76 Å). The other possible site differs only by having one of the Cl atoms replaced by OH^-, but located at a shorter distance (2.35 Å). In paratacamite, there are also two possible octahedral sites for the Cu atoms. One consists of Cu surrounded by four OH^- (planar) at a shorter distance (2.0 Å) with two Cl atoms further away (2.4 Å). The second site has Cu surrounded by six OH^- at 2.12 Å. Hence, we can conclude that such Cu sites in $Cu_2(OH)_3Cl$ would be very distinct when analyzed by a technique sensitive to the short-range order, such as XANES and XPS.

Therefore, we may ascertain that in the case of Reaction-I additional atacamite Cu sites were formed. The XANES collected at the end of this reaction shows a well pronounced feature in the absorption edge (named *C*), which is associated with a distortion in the octahedral site due to the existence of different interatomic distances. This same structure is not observed in the XANES of the final spectrum of Reaction-II, indicating the formation of regular octahedra. Such regularity in the short range is observed in the structure of paratacamite. In addition, paratacamite has a larger number of Cu–O bonds compared with atacamite, and this was observed effectively by XPS analysis of the particles formed by Reaction-II.

5. Conclusions

We were able to monitor the evolution of the structural and electronic properties of the Cu atoms during the formation of copper trihydroxyl chloride [$Cu_2(OH)_3Cl$] particles in an aqueous solution, at room temperature. Both reactions resulted in the formation of a mixture of two $Cu_2(OH)_3Cl$ polymorphs: atacamite and paratacamite. Although the formed particles presented very similar crystalline structures in the long-range order (as observed by XRD), the *in situ* DXAS indicated dramatic local order differences around the copper atoms. The presence of PVP in Reaction-I induced the formation of more ordered $Cu_2(OH)_3Cl$ with a larger number of atacamite Cu sites, whereas the absence of PVP in Reaction-II resulted in fewer crystalline particles with a larger number of patacamite Cu sites. The PVP also contributes to the avoidance of the reduction of the precursor from $CuCl_2$ (Cu^{2+}) to CuCl (Cu^+), which was found in Reaction-II. The chemical bonds observed by the synchrotron-radiation XPS corroborated the XANES findings. The proposed method of synthesis is more efficient and environmentally friendly compared with similar reported methods, but it has the additional advantage of working at lower temperatures.

The instrumentation built for the *in situ* studies presented an important contribution to this work. The development of the reactor was focused on its use for *in situ* DXAS measurements, aiming at a simple design that enables data collection of a given liquid phase reaction with temporal resolution. The reactor demonstrated excellent performance and its application may be extended to investigate other systems, either for EXAFS or XANES *in situ* experiments.

This work has been supported by the Brazilian Synchrotron Light Laboratory (LNLS) under the proposals DXAS-8768, DXAS-8150 and SXS-7648. Financial support from CNPq and FAPERGS is also acknowledged. The authors would like to thank the CME-UFRGS and CNANO for SEM measurements, the LNLS staff, and Professor F. Bernardi, J. Alexandre, D. C. A. Ribeiro for valuable contributions in sample preparation and characterization. JB thanks CNPq for his PhD fellowship.

References

Adriaens, A., Dowsett, M., Jones, G., Leyssens, K. & Nikitenko, S. (2009). *J. Anal. At. Spectrom.* **24**, 62.
Bernardi, F., Alves, M. C. M. & Morais, J. (2010). *J. Phys. Chem. C*, **114**, 21434–21438.
Cartier, C. (1988). PhD thesis, Université Paris Sud, Centre d'Orsay, France.
Chen, J., Deng, S. Z., Xu, N. S., Zhang, W., Wen, X. & Yang, S. (2003). *Appl. Phys. Lett.* **83**, 746.
Chowdhuri, A., Gupta, V., Sreenivas, K., Kumar, R., Mozumdar, S. & Patanjali, P. K. (2004). *Appl. Phys. Lett.* **84**, 1180.
Dowsett, M. G., Adriaens, A., Jones, G. K. C., Poolton, N., Fiddy, S. & Nikitenko, S. (2008). *Anal. Chem.* **80**, 8717–8724.
Fleet, M. E. (1975). *Acta Cryst.* B**31**, 183–187.
Han, M. S., Lee, B. G., Ahn, B. S., Kim, H. S., Moon, D. J. & Hong, S. I. (2003). *J. Mol. Catal. A*, **203**, 137–143.
Jia, W., Reitz, E., Sun, H., Li, B., Zhang, H. & Lei, Y. (2009). *J. Appl. Phys.* **105**, 064917.
Koningsberger, D. C. & Prins, R. (1988). Editors. *X-ray Absorption: Principles, Applications, Techniques of EXAFS, SEXAFS and XANES. Chemical Analysis: A Series of Monographs on Analytical Chemistry and Its Applications*, Vol. 92. New York: Wiley and Sons.
Lee, S., Park, S., Lee, S., Lee, J. & Kim, H. (2007). *Catal. Today*, **120**, 358–362.
Nishimura, S., Takagaki, A., Maenosono, S. & Ebitani, K. (2009). *Langmuir*, **26**, 4473–4479.
Park, B. K., Kim, D., Jeong, S., Moon, J. & Kim, J. S. (2007). *Thin Solid Films*, **515**, 7706–7711.
Tamaki, J., Shimanoe, K., Yamada, Y., Yamamoto, Y., Miura, N. & Yamazoe, N. (1998). *Sens. Actuators B*, **49**, 121–125.
Tolentino, H. C. N., Cezar, J. C., Watanabe, N., Piamonteze, C., Souza-Neto, N. M., Tamura, E., Ramos, A. Y. & Neueschwander, R. (2005). *Phys. Scr.* T**115**, 977–979.
Tolentino, H., Compagnon-Cailhol, V., Vicentin, F. C. & Abbate, M. (1998). *J. Synchrotron Rad.* **5**, 539–541.
Wang, H., Pan, Q., Zhao, J., Yin, G. & Zuo, P. (2007). *J. Power Sources*, **167**, 206–211.
Zheng, X. G., Xu, C. N., Tomokiyo, Y., Tanaka, E., Yamada, H. & Soejima, Y. (2000). *Phys. Rev. Lett.* **85**, 5170–5173.